 doi:10.20944/preprints202210.0358.v1

Article

A Modified single frequency PPP method for the Positioning and Time transfer with BDS−3

Mingjun Ouyang [1,*], Xiangwei Zhu [1,*], Junzhi Li [1], Yang Liu [2]

1. School of Electronics and Communication Engineering, Sun Yat-Sen University, Guangzhou, 510006, China;
2. School of Aeronautics and Astronautics, Sun Yat-Sen University, Guangzhou 510006, China

* Correspondence: ouymj@mai2.sysu.edu.cn, zhuxw666@mail.sysu.edu.cn

Abstract: In this paper, four types of open service signals of BDS-3 satellite (B1I, B1C, B2a, and B3I) and B2I signals broadcasted by BDS-2 satellites were used in the time frequency transfer and positioning experiments with signal coexisting in BDS system, and the single frequency PPP (precise point positioning) method was used. Modified GRoup And PHase Ionospheric Correction (GRAPHIC) method was proposed and verified by the experiment. The results show that 18 selected stations can achieve decimeter-level positioning results with single frequency. Compared with the general observation method, the proposed modified GRAPHIC method improves the stability and precision of positioning and timing significantly, and the positioning accuracy of 5 frequency signals is increased 40.4%, 32.2%, 80.3%, 12.4%, and 10.3%, respectively. The frequency stability can reach the same accuracy as that of dual-frequency with BDS in the current state.

Keywords: BDS-3; Time transfer; Precise point positioning; Single frequency; Group and Phase Ionospheric Correction (GRAPHIC)

1. Introduction

The construction process of the BDS-3 started in 2015. Different from the regional service provided by the BDS-2, the BDS-3 includes 3 GEO (Geostationary Earth Orbit), 24 MEO (Medium orbit earth satellite), and 3 IGSO (Inclined GeoSynchronous Orbit) satellites, which can provide global service（Yang et al., 2019). During the launch of the BDS-3 experimental satellites and after the launch of some BDS-3 satellites, much research on BDS-3 determination of satellite orbit, estimation of clock difference, positioning, time and frequency transfer, and other related subjects has been conducted. In 2018, Li et al. performed the determination of orbit on the BDS-3, by using the MGEX (The Multi-GNSS Experiment and Pilot Project) and iGMAS (international GNSS Monitoring & Assessment System) stations（Li et al., 2019). Zhang et al. conducted a statistical study on the new signals (B1I, B1C, B2a, B2b, and B3I) generated by the BDS-3 in terms of the signal-to-noise ratio, multipath etc.（Zhang et al., 2017). Ye et al. determined the BDS-3 satellite orbit by using B1C and B2a frequency signals（Ye et al., 2018). Yan et al. determined the exact clock difference and orbit of the BDS-3（Yan et al., 2019). Xie et al. conducted the orbit determination by analysis of a BDS-3 satellite in L and Ka bands（Xie et al., 2019). Yang et al. introduced the coordinate system, time system overall design of the BDS-3 system in detail, and first presented the signal-in-space ranging errors (SISRE) results of eight BDS-3 satellites in four days, and compared the broadcast ephemeris and precise orbit results. The results showed that the root mean square (RMS) of the three-dimensional (3D) satellite orbit was about 1.07 m, the average RMS of the satellite clock difference was 1.12 ns, and the average SISRE was 0.44 m（Yang et al., 2019). Zhang et al. studied on positioning by using the new signal, and found that the accuracy level of the Single Point Positioning (SPP) of the new BDS-3 signal was equivalent to that of the GPS（Zhang et al., 2019).

Preprints (www.preprints.org) | NOT PEER-REVIEWED | Posted: 24 October 2022 doi:10.20944/preprints202210.0358.v1

Ge et al. evaluated the performance of the BDS-2 dual-frequency ionosphere-free (IF) combination in terms of time frequency transfer by using the iGMAS product（Ge et al., 2019). Tu et al. found that there was lower observation noise and could achieve the same accuracy of time transfer as the GPS by using the triple frequency un-differenced and un-combined (UC)（Tu et al., 2019). Zhang et al. evaluated the GPS PPP using different institutional products and systems, obtained that the time transfer accuracy of sub-nanosecond（Zhang et al., 2019). Ge et al. evaluated the time frequency transfer of the BDS-3 through experiments with different combinations（Ge et al., 2020), and got the conclusion that the stability and accuracy of new signal perform better.

However, all the above-mentioned research, whether it is related to the orbit determination and the calculation of clock difference, or positioning and application research of time frequency transfer, all of them were based on the multi-frequency signals of BDS-3, and did not considered the needs of single frequency users, which is the largest user group of the GNSS currently. At present, GNSS navigation chips was built in almost all smartphones to meet the navigation and positioning needs of consumers. Studying the performance of a single frequency algorithm can help to improve and expand the application scope and depth of the consumer market.

At present, BDS-2 and BDS-3 coexist in the sky, and can be regarded as the same system or different system, when positioning and other applicating. In this paper, the BDS-2 was used as a benchmark, and the BDS-3 was used as a different system in the program design. This paper proposes a modified single frequency GRAPHIC model. As the ionospheric refraction correction of code pseudo-range and carrier phase observations are equal in size, but opposite in sign, a method of ionosphere free is formed between the code and carrier phase observations. Based on the two algorithms of the single frequency model (single frequency UC model, and single frequency modified GRAPHIC model), this paper studies the positioning and time frequency transfer, and evaluates the performance of current single frequency coexist of BDS-2 and BDS-3 by PPP method.

The rest of the paper is organized as follows. Section 2 introduces the current BDS-3 status in detail. Section 3 explains the two main single frequency algorithms used in this work. Section 4 presents the detailed processing strategy and data selection. Section 5 analyzes and compares the results. Section 6 draws and summarizes relevant conclusions.

2. Current BDS-3 status

According to the three-steps strategy, the BDS moves from the second generation of the regional system to the third generation of the global system. After the successful launch of the last BDS-3 networking satellite on June 23, 2020, the BDS has officially become a global satellite navigation system and completed the construction tasks of third generation.

15 satellites of the BDS-2 system operate continuously and stably in at present. Before the networking of the BDS-3 system formally, 5 BDS-3 experimental satellites were launched and verified by on orbit tests. Higher performance rubidium atomic clocks (with daily stability of 10E-14 magnitude) and hydrogen atomic clocks (with daily stability of 10E-15 magnitude) were developed, which modified the performance and service life of the satellite further. A stable and reliable inter satellite link was built, and the basic system constellation deployment has been completed successfully. BDS-3 has realized the integration design of navigation and positioning, communication, and enhanced services. In addition to navigation and positioning, it also provides 6 types of services, including satellite-based enhancement, precise positioning information broadcast, regional short message, global short message, communication, and international search and rescue（Yang et al., 2019).

Table 1. Signal characteristics of BDS-3 open service

Frequency band	Signal component	Center frequency (MHz)	Modulation mode	Information rate / BPS	Compatible interoperability
B1	B1C_data	1575.42	BOC(1,1)	50	GPS L1

Preprints (www.preprints.org) | NOT PEER-REVIEWED | Posted: 24 October 2022 doi:10.20944/preprints202210.0358.v1

	B1C_pilot		QMBOC(6,1,4/33)	0	Galileo E1
	B1I	1561.098	BPSK(2)	50(MEO/IGSO),500(GEO)	--
B2	B2a_data	1176.45	QPSK(10)	100	GPS L5
	B2a_pilot			0	Galileo E5a
	B2b_I	1207.14	QPSK(10)	500	Galileo E5b
	B2b_Q			500	
B3	B3I	1268.52	BPSK(10)	50(MEO/IGSO),500(GEO)	--

BDS-3 is downward compatible with BDS-2 B1I and B3I signals, and two new signals B1C and B2a (compatible with GPS L1/L5 and Galileo E1/E5A) are added to provide public navigation signals with four frequencies（Lu et al., 2019). B1C and B2a signals have wider bandwidth, higher ranging accuracy and better interoperability compared with conditional signals. Pilot channels are generally added to increase the receiving sensitivity of weak signals, and LDPC (Low-density Parity-check) channel coding is used to improve the demodulation performance of weak signals (as shown in Table 1). B1C and B2a also modulate new navigation messages BGCNAV1 and BGCNAV2, and adopt new orbit parameters and new global ionospheric model BDGIM (BeiDou Global Ionospheric delay correction Model) based on spherical harmonic function. The accuracy of orbit and ionospheric correction are modified significantly than that of BDS-2（Yuan et al., 2019). Since the service of BDS-2 satellite would continue many years, BDS-2 and BDS-3 coexist at present. Therefore, this paper studies the application of single frequency PPP method in the coexistence state of two generations of systems, which is of great significance to the majority of consumers.

3. Principle and improvement of single frequency PPP algorithm

3.1. Basic formula

The observation data can be expressed as follows:

$$P_{r,j}^{s} = \rho_r^s + c \cdot dt_r^s - c \cdot dt^s + MF_w(e) \cdot \mathrm{Z}_w + \gamma_j^s \cdot I_{r,1}^s + (d_{r,j}^s - d_j^s) + \varepsilon_{r,j}^s(P) \tag{1}$$

$$\Phi_{r,j}^{s} = \rho_r^s + c \cdot dt_r^s - c \cdot dt^s + MF_w(e) \cdot \mathrm{Z}_w - \gamma_j^s \cdot I_{r,1}^s + \lambda_j^s \cdot (N_{r,j}^s + b_{r,j}^s - \mathrm{b}_j^s) + \varepsilon_{r,j}^s(\varphi) \tag{2}$$

where r, j, and s stand for receivers, frequency, and satellite systems, respectively; $p_{r,j}^s$ and $\Phi_{r,j}^s$ represent the pseudo-range observation and the carrier phase observation, respectively; λ_j^s denotes the wavelength of frequency j; ρ_r^s represents the geometric distance between receiver and satellite; c represents the speed of light; dt_r^s and dt^s denote the receiver clock difference and the satellite clock difference, respectively; e represents the elevate angle of a satellite; $MF_w(e)$ denotes the wet delay projection function; Z_w refers to the wet delay of zenith direction, $I_{r,1}^s$ represents the tilt direction delay of ionosphere; multiple factor $\gamma_j^s = (f_1^s / f_j^s)^2$ is based on frequency; $d_{r,j}^s$ and d_j^s represent uncalibrated code delays (UCDs) at receiver and satellite, respectively; $N_{r,j}^s$ represents the integer ambiguity, $b_{r,j}^s$ and d_j^s denote uncalibrated carrier phase delays (UPDs) at receiver and satellite, respectively; lastly, $\varepsilon_{r,j}^s(P)$ and $\varepsilon_{r,j}^s(\varphi)$ represent the carrier phase noise and the pseudo-range noise, respectively.

3.2. Single frequency UC PPP model

For the dual-frequency ionosphere free, the first order ionosphere has been eliminated, that is, more than 99.9% of the ionospheric error has been eliminated. For a single frequency, the delay of

Preprints (www.preprints.org) | NOT PEER-REVIEWED | Posted: 24 October 2022 doi:10.20944/preprints202210.0358.v1

ionosphere can be used only as parameter to estimate or model to be corrected, or external precision products.

The satellite clock difference of precision products is estimated using the combination of P1 and P2 pseudo ranges. Therefore, satellite clock (d^s_{IF12}) represents a combination of satellite UCDs ((d^s_{IF12})) and actual clock difference dt^s , which is expressed as follows:

$$c \cdot dt^s_{IF12} = c \cdot dt^s + (\alpha^2_{12} \cdot d^s_1 + \beta^2_{12} \cdot d^s_2) \tag{3}$$

where $\alpha^s_{12} = \frac{(f^s_1)}{(f^s_1)^2 - (f^s_2)^2}$ and $\beta^s_{12} = -\frac{(f^s_2)}{(f^s_1)^2 - (f^s_2)^2}$.

The clock difference from broadcast ephemeris of the BDS corresponds to the B3I frequency point (CSNO (2018a) BeiDou Navigation satellite system signal in space interface control document open service signal B3I (Version 1.0), 2018), while the precise clock difference corresponds to the B1I/B3I ionosphere free combination (Wang et al., 2019). Therefore, TGD (Time Group Delay) or DCB (Differential Code Biase) should be used to correct the single frequency solution or other combined solution as show in Figure 1. The specific correction methods are presented in (Ge et al., 2017) (Montenbruck et al., 2017). In this study, the DCB correction provided by the Institute of Geodesy and Geophysics (IGG), Chinese Academy of Sciences, including the GPS, GLONASS, Galileo, BDS, and QZSS, with an accuracy of range from 0.2ns to 0.6 ns (Wang et al., 2017).

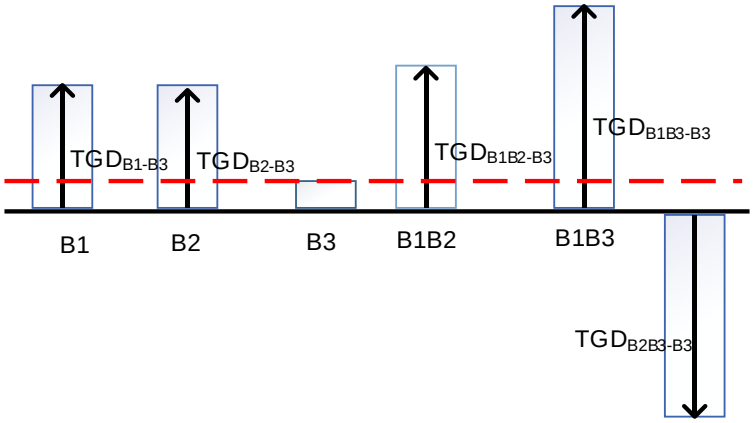

Figure 1. Presentation of the TGD relationship.

In this paper, the COD precision clock product was used. After using the precision clock difference product, equations (1) and (2) are linearized, and formula (3) is substituted into equations (4):

$$\begin{cases} p^s_{r,1} = \mu^s_r \cdot x + c \cdot dt_r + d^s_{r,1} + MF_w(e) \cdot Z_w + I^s_{r,1} - \beta^s_{12} \cdot DCB^s_{P1P2} + \varepsilon^s_{r,1}(P) \\ l^s_{r,1} = \mu^s_r \cdot x + c \cdot dt_r - I^s_{r,1} + d^s_{IF12} + MF_w(e) \cdot Z_w + \lambda^s_1 \cdot (N^s_{r,1} + b^s_{r,1} - b^s_1) + \varepsilon^s_{r,1}(\varphi) \end{cases} \tag{4}$$

where $p^s_{r,1}$ and $l^s_{r,1}$ represent the calculated value of observation value minus pseudo range and carrier phase observation, respectively; x is the unit vector between receiver and satellite, denoted the position vector relative to a prior coordinate position, and the other parameters are the same as defined for equations (1) and (2).

3.3. Modified GRAPHIC PPP model

The GRAPHIC method was proposed by Yunck in 1993. By using the characteristics of ionospheric delay and carrier phase, which are equal in size, but opposite in sign, to eliminate the

Preprints (www.preprints.org) | NOT PEER-REVIEWED | Posted: 24 October 2022 doi:10.20944/preprints202210.0358.v1

influence of ionospheric delay, the noise of the equation is reduced by half, and the convergence speed of the PPP is increased by 20% (Gao et al., 2017). According to equations (1) and (2), the modified GRAPHIC of single PPP model can be expressed as:

$$\begin{cases} L_{r,1}^{s} = 1/2 \cdot (p_{r,j}^{s} + l_{r,1}^{s}) = \mu_r^s \cdot x_{r,1}^{s} + c \cdot dt_r + MF_w(e) \cdot \mathrm{Z}_w + 1/2 \cdot \lambda_1^s \cdot N_{r,1}^{s} + B_{r,1}^{s} + \varepsilon_{r,1}^{s}(L) \\ p_{r,1}^{s} = \mu_r^s \cdot x + c \cdot dt_r + d_{r,1}^{s} + MF_w(e) \cdot \mathrm{Z}_w + I_{r,1}^{s} - \beta_{12}^{s} \cdot DCB_{P1P2}^{s} + \varepsilon_{r,1}^{s}(P) \end{cases} \tag{5}$$

$$B_{r,1}^{s} = 1/2 \cdot d_{r,1}^{s} + 1/2 \cdot d_{IF12}^{s} - 1/2 \cdot \beta_{12}^{s} \cdot DCB_{P_1P_1}^{s} + 1/2(b_{r,1}^{s} - b_1^{s}) \tag{6}$$

In order to prevent rank deficiency, in equation (5), the pseudo-range observation equation is added, and the ionospheric delay was corrected by using ionospheric products this equation. The clock difference parameters are sorted out, which is expressed as:

$$\begin{cases} c \cdot \bar{dt}_r = c \cdot dt_r + B1_{r,1}^{s} \\ \overline{N}_{r,1}^{s} = \lambda_1^s \cdot N_{r,1}^{s} + \delta B_{r,1}^{s} \end{cases} \tag{7}$$

where $B1_{r,1}^{s}$ represents the average delay, and $\delta B_{r,1}^{s}$ denotes the delay of the satellite, which will be absorbed into the ambiguity parameter and the satellite clock difference parameter. The final estimated parameter vector $\overline{X}$ is expressed as:

$$\overline{X} = \begin{bmatrix} x & \bar{dt}_r & Z_w & \overline{N}_{r,1}^{s} \end{bmatrix} \tag{8}$$

It should be noted that in the newly constructed function model, the pseudo-range and GRAPHIC equations in (5), Both used pseudo-range observations, so there is a correlation between the combined observations. In this paper, a stochastic model is constructed based on the covariance propagation law. Suppose $\hat{\sigma}_{P_1} = \hat{\sigma}_{P_2} = \hat{\sigma}_P$, $\hat{\sigma}_{\Phi_1} = \hat{\sigma}_{\Phi_2} = \hat{\sigma}_\Phi$, then the corresponding satellites are obtained from the error propagation law, and the values of each position of the covariance matrix are:

$$\begin{cases} P_{IF,Li} = 0.5(P_i + \Phi_i) \\ Q_{Pi,Pi} = \hat{\sigma}_P^2 \\ Q_{UofC,UofC} = 0.25\hat{\sigma}_P^2 + 0.25\hat{\sigma}_\Phi^{\ 2} \\ Q_{Pi,UofC} = 0.5\hat{\sigma}_P \end{cases} \tag{9}$$

4. Data selection and processing

4.1. Data selection

Some MGEX tracking stations have the ability to track signals of BDS-3. In order to verify the feasibility of a single frequency algorithm and to simulate the performance of global distribution, this paper selects 18 MGEX sites for positioning experiment, as shown in Figure 2. Some of the stations are connected high-precision atomic clocks, which can be used for high-precision time frequency transfer research.

Preprints (www.preprints.org) | NOT PEER-REVIEWED | Posted: 24 October 2022 doi:10.20944/preprints202210.0358.v1

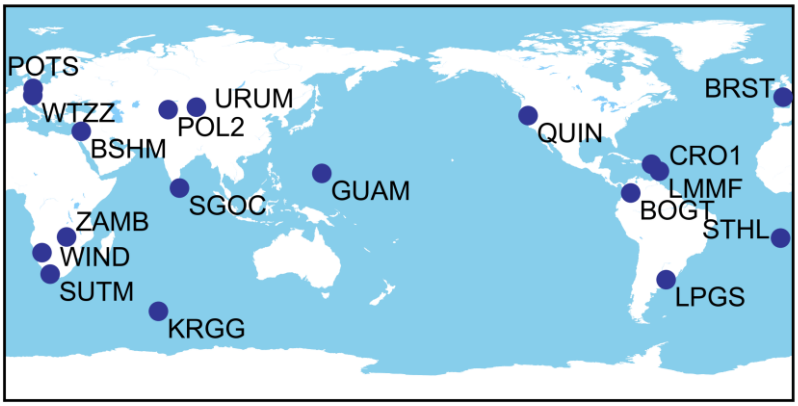

Figure 2. Distribution of selected stations.

The data was collected on April 9, 2020 (DOY 100,YEAR2020), and the sampling rate was 30 seconds. The public service data (B1I, B1C, B2I, B2a, and B3I) of the BDS-3 and BDS-2 could be received. Three stations, CUSV, HARB, and WTZZ, were selected for time transfer experiment with the external atomic clock. Two time-links, WTZZ-HARB and WTZZ-CUSV, were formed with WTZZ as the center.

4.2. Strategy design and filtering algorithm

In this paper, two kinds of single frequency PPP strategies are designed and compared: single frequency PPP UC strategy (denoted as strategy 1) and modified single frequency GRAPHIC strategy (denoted as strategy 2). Detailed strategy of PPP algorithm was given in Table2.

Table 2. Detailed strategy of PPP algorithm

Parameter	Description
Wet tropospheric delay	UNB3 model (Collins et al., 1997)
Signal selection	（B1I, B1C,B2I, B2a, B3I）
Satellite antenna PCO and PCV	Igs14.atx
Elevation cut off	7°
Solid earth tides	IERS Conventions 2010 (Petit et al., 2010)
Ocean loading	IERS Conventions 2010 (Petit et al., 2010)
Polar tides	IERS Conventions 2010 (Petit et al., 2010)
Phase wind-up effect	Wu model (Wu et al., 1992)
Receiver clock errors	Estimation, white noise
Station coordinate	Static model
Estimator	Kalman filter

5. Results and analysis

The two single frequency PPP methods were compared and analyzed in detail based on the positioning of the existing frequency. In the following text, some graphs marked with *U* relate to the UC methods, and those marked with *G* relate to the modified GRAPHIC.

5.1.Positioning results

As mentioned previously, the BDS-3 is a global navigation system. Compared with the BDS-2, its visible satellite number and PDOP value of sites in all regions of the world are significantly

Preprints (www.preprints.org) | NOT PEER-REVIEWED | Posted: 24 October 2022 doi:10.20944/preprints202210.0358.v1

modified, which means the needs of all types of users in the world. Jiang et al. (Jiang et al., 2019) derived the statistics of the PDOP value of the BDS-2 + BDS-3 , and pointed out that increasing the signal is helpful to improve the performance of PDOP value outside the Asia Pacific region . The last BDS-3 satellite was launched on June 23, 2020, which completed the global networking. Its satellite visibility and PDOP value are comparable to the GPS system in the global scope. Even in the Asia Pacific, Australia, and some other regions, due to the unique GEO and IGSO of the BDS, its satellite visibility and PDOP value will be better than those of the GPS system. In the 60°S – 60°N and 50°E – 170°E regions, BDS-3 has 11 to 14 visible satellites, which is larger than the GPS and Galileo systems with range from 1 to 3, respectively, and larger than the GLONASS with range 3 to 7 (Wang et al., 2019).

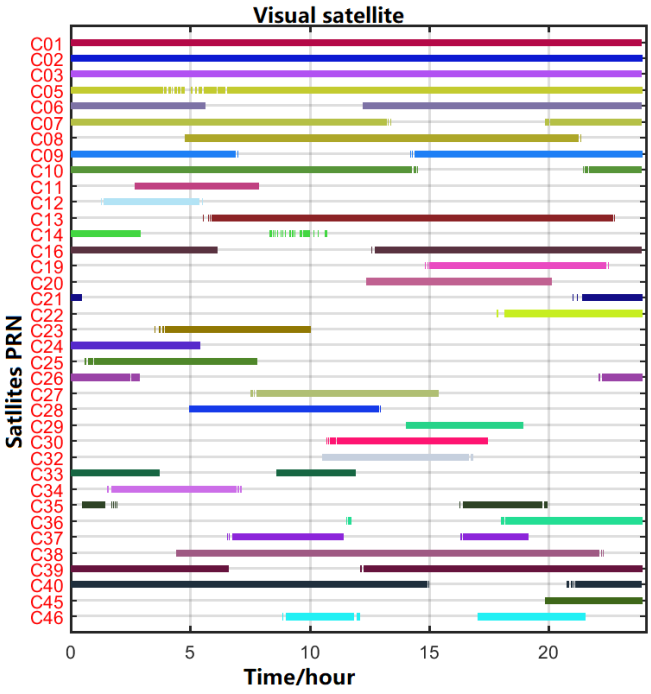

Figure 3. Satellite visibility of the WUH2 station and BDS satellite on 2020/04/09.

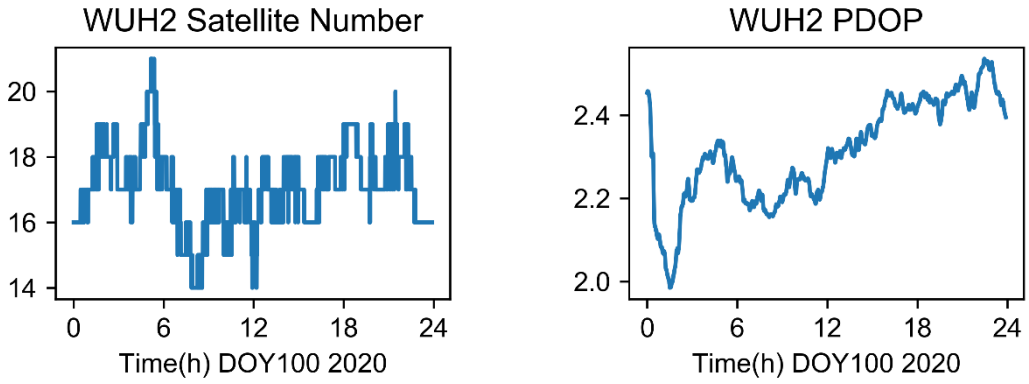

Figure 4. The visible satellite number and PDOP value of the WHU2 station and BDS satellite.

Figure 3 shows the visible satellite number and PDOP value of a domestic station WUH2 used in the experiment at (DOY 001, 2020). In Figure 3, it can be seen that the average number of visible satellites in a day was more than 16, and the PDOP value was approximately 2.2, which could better meet the application requirements of positioning, time frequency transfer, tropospheric solution, etc.

Preprints (www.preprints.org) | NOT PEER-REVIEWED | Posted: 24 October 2022 doi:10.20944/preprints202210.0358.v1

A large number of redundant satellites and a good PDOP value can be helpful for the user to achieve the continuousness and robust of algorithm.

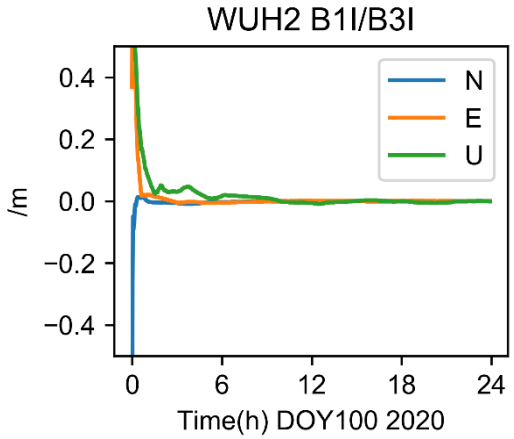

Figure 5. BDS B1I/B3I ionospheric free results of WUH2

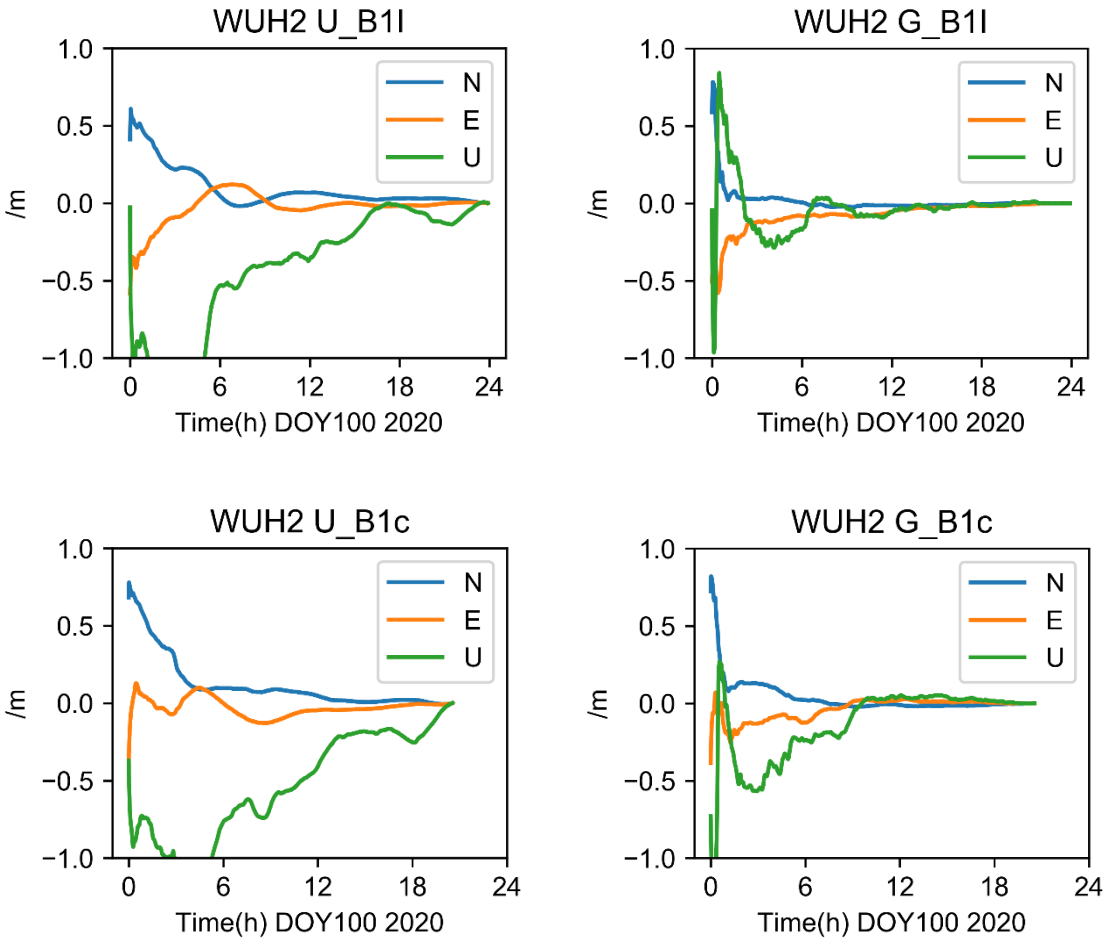

Preprints (www.preprints.org) | NOT PEER-REVIEWED | Posted: 24 October 2022 doi:10.20944/preprints202210.0358.v1

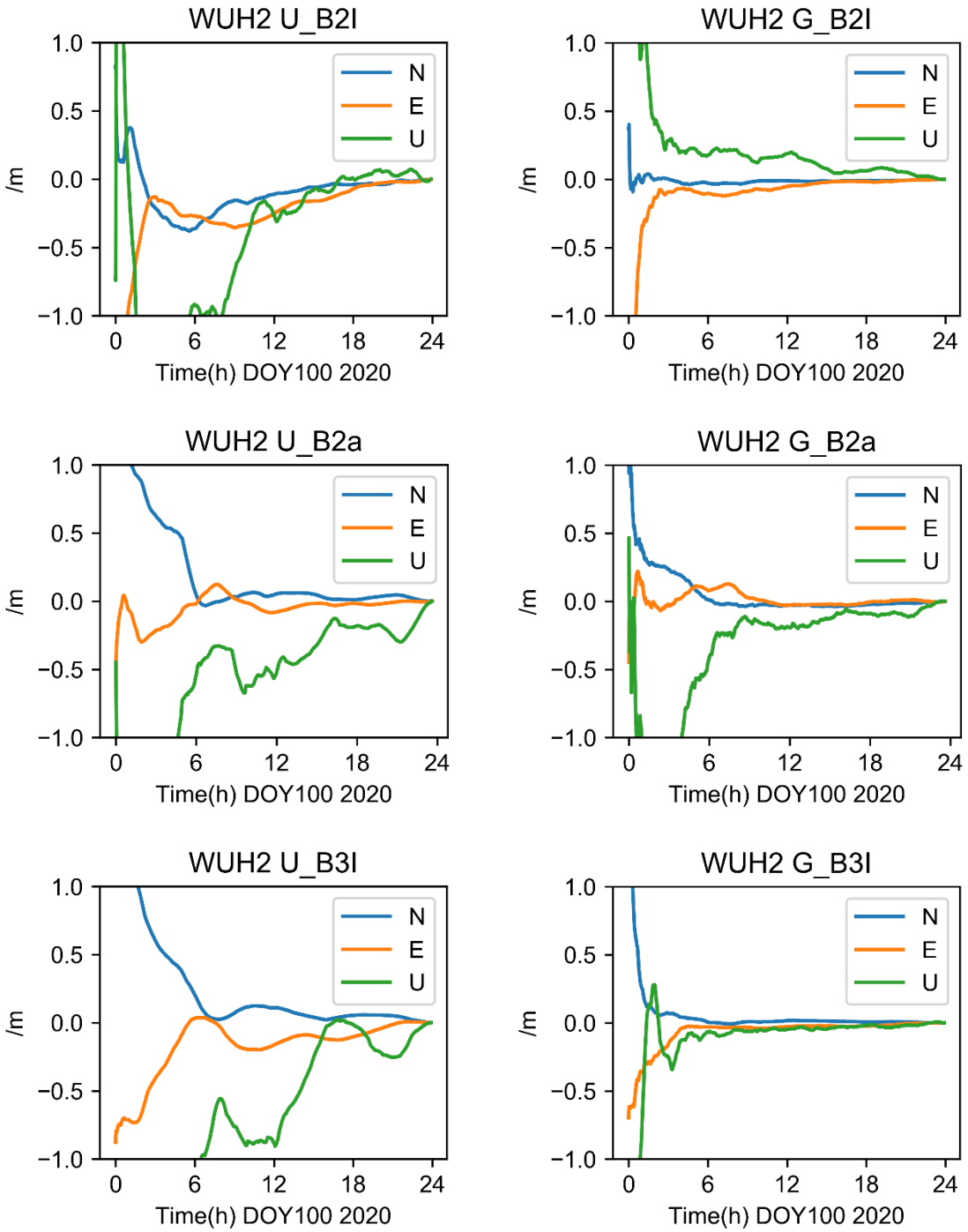

Figure 6. Positioning results of single frequency algorithms at 5 frequency (strategy1, strategy 2).

The combination of BDS BI1 and B3I dual-frequency ionosphere free was taken as a reference in the positioning experiment in Figure 5. The precise orbit and clock difference product used in this work was COD. Its satellite clock difference product was based on the combination of B1I and B3I frequency, so the satellite clock doesn't need to be modified by the DCB. Fig. 5 shows the positioning results of the dual-frequency of the WHU2 station, where it can be seen that the accuracy in horizontal directions E and N, reached millimeter level, while the vertical direction U was slightly poor, but it was at centimeter level after the convergence.

Figure 6 shows the positioning results of station WUH2 obtained by the single frequency UC (strategy 1) and modified GRAPHIC (strategy 2). The results show that in three directions (E, N, U),

Preprints (www.preprints.org) | NOT PEER-REVIEWED | Posted: 24 October 2022 doi:10.20944/preprints202210.0358.v1

the positioning accuracy was at decimeter level after the convergence. Due to the absence of ionosphere constraints, some results appeared to be systematic biases. The overall accuracy of U in vertical direction is worse than that in horizontal directions (N and E).

For 5 frequency, the positioning accuracy and stability of the strategy 2 was better than that of strategy 1. The result of the B1C frequency was interrupted for 2 hours as the reason that the receiver decoded data abnormally, which resulted in data loss.

In order to further verify and analyze the above conclusions, 18 stations (as shown in Figure 3) distributed in the global were used in the average statistical comparison. Figures 7 and 8 show the positioning results of each frequency point of 18 stations with strategy 1 and strategy 2, respectively. Figure 9 shows the overall positioning results of 18 stations from the point of view of each frequency.

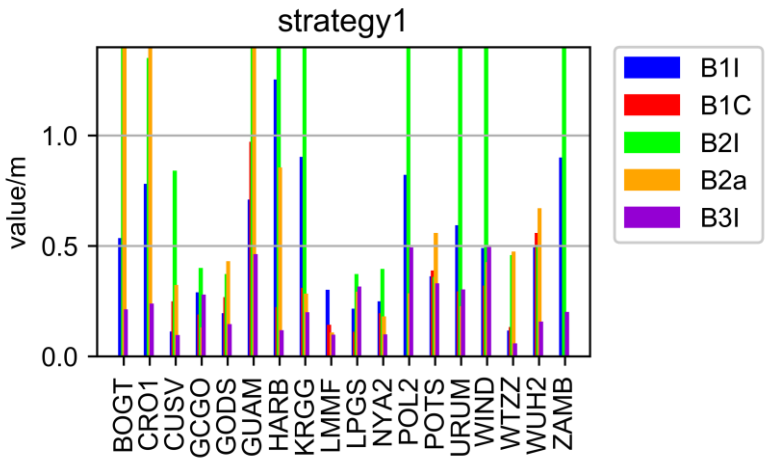

Figure 7. The results of strategy 1.

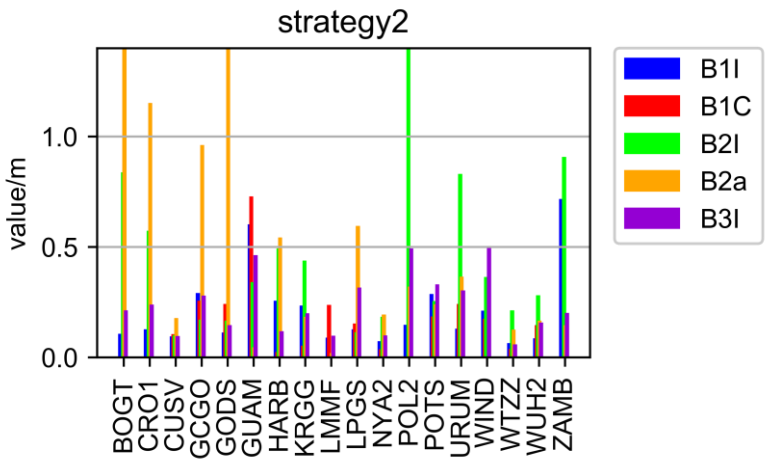

Figure 8. The results of strategy2.

As presented in Figures 7 and 8, the positioning accuracy of all stations and all frequency, except for some stations of B1I/B2a/B2I signal, strategy 2 was less than 0.5 decimeter, while that of the strategy 1 was less than 0.75 decimeter. The poor performance of the B2I was due to the fewer number of satellites. Only BDS-2 transmitted B2I, and the number of satellites was even less than 4 at some times in some areas. The positioning results of B1C and B3I were obviously better than other frequency. The preliminary analysis showed that there were more satellites, and the data quality was better.

Preprints (www.preprints.org) | NOT PEER-REVIEWED | Posted: 24 October 2022 doi:10.20944/preprints202210.0358.v1

In Figure 9, the average position value of 18 stations is shown from the point of view of each frequency. The positioning results of the strategy 2 are better than strategy 1, and the frequency B1I, B1C, B2I, B2A, and B3I are increased by 40.4%, 32.2%, 80.3%, 12.4%, and 10.3%, respectively, compared with strategy 1.

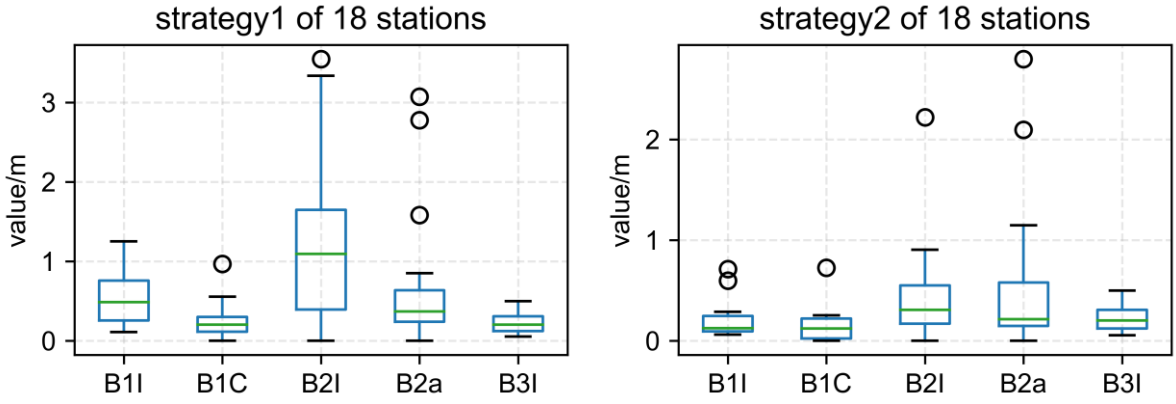

Figure 9. Average position value of 18 stations

5.2. Comparison of time and frequency transfer

The old and new single frequency BDS signals (B1I, B1C, B2I, B2a, B3I) were tested in high-precision time frequency transfer. Three MGEX stations (CUSV, WTZZ, HARB) were selected, all of which were externally connected with high-precision atomic clocks. Based on the CUSV, two time transfer links (CUSV-WTZZ, CUSV-HARB) were formed. In reference [11], it has been proven that the combination of B1I and B3I ionosphere free of BDS-3 can achieve the time transfer accuracy of the corresponding strategy using the GPS system. Therefore, B1I and B3I ionospheric free of BDS was adopted as a reference. Due to the system deviation between single frequency and double-frequency combination, the STD method was used for statistical comparison. In addition, the modified Allan variance was used for analysis and comparison of frequency stability of the time-links.

STD is the arithmetic square root of variance, also known as mean square error in formula 10. It is the average of the distance of each data deviating from the average. It is the square root after averaging the square sum of mean deviation. The standard deviation can reflect the dispersion degree of a data set.

X_i is the clock error or clock links obtained by the single frequency method minus the reference clock error or clock links of IF method. N is the number of all clock difference sequence points. $\overline{X}$ is average value of X_i .

$$STD=\sqrt{\frac{\sum_{i=1}^{N}(X_i-\overline{X})^2}{N}} \tag{10}$$

5.2.1 Clock difference result

Figure 10 shows the clock difference statistics STD results of two strategies of three stations (CUSV, HARB, WTZZ). It can be seen that the clock difference statistics STD of strategy 2 is significantly smaller than strategy 1, which means that strategy 2 is very helpful to improve clock error accuracy compared with strategy 1.

Figure 11 shows that the STD of three stations can be stabilized at the sub-nanosecond order by using the single frequency GRAPHIC method (strategy 2). When the strategy 2 was used, the clock

Preprints (www.preprints.org) | NOT PEER-REVIEWED | Posted: 24 October 2022 doi:10.20944/preprints202210.0358.v1

difference parameter was more stable and accurate than when the UC method (strategy 1). The performance of new signal B1C was obviously better than other frequency signals. However, this is the result of only three stations, and more stations are needed to verify this result, which is out of the scope of this paper. Due to the fewer number of B2I satellites, the performance of B2I is significantly worse than of the other frequency.

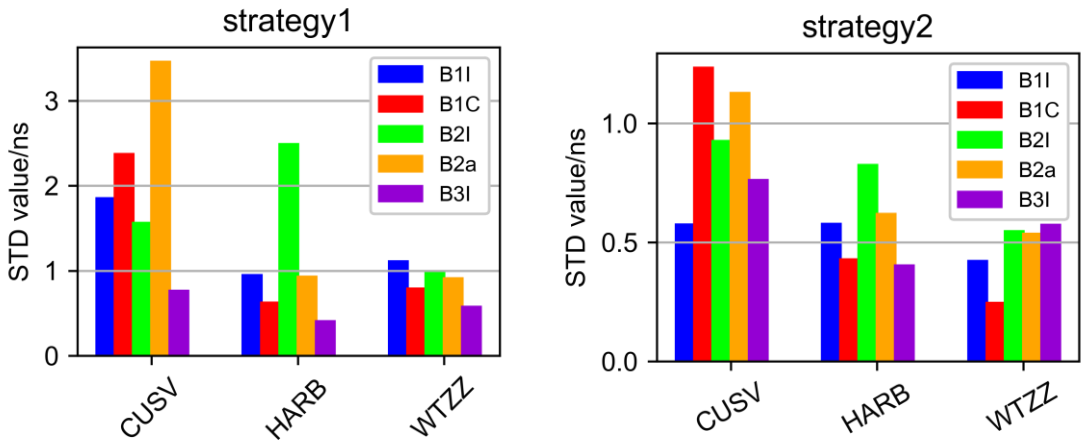

Figure 10. The results of clock difference statistics STD of two strategies of three stations (CUSV, HARB, WTZZ).

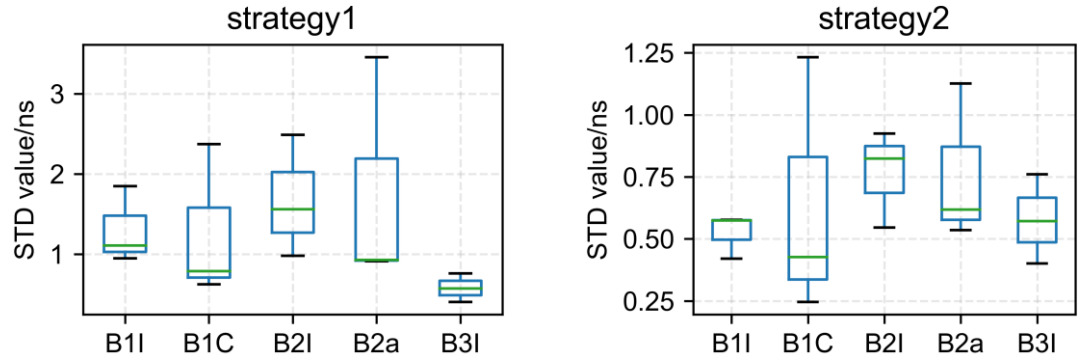

Figure 11. The average STD of clock difference of three stations with two strategies for different frequency points.

5.2.2 Time-links result

Preprints (www.preprints.org) | NOT PEER-REVIEWED | Posted: 24 October 2022 doi:10.20944/preprints202210.0358.v1

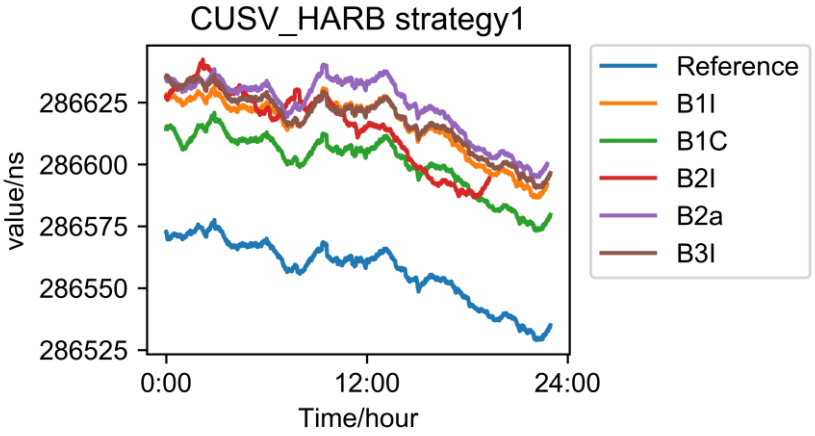

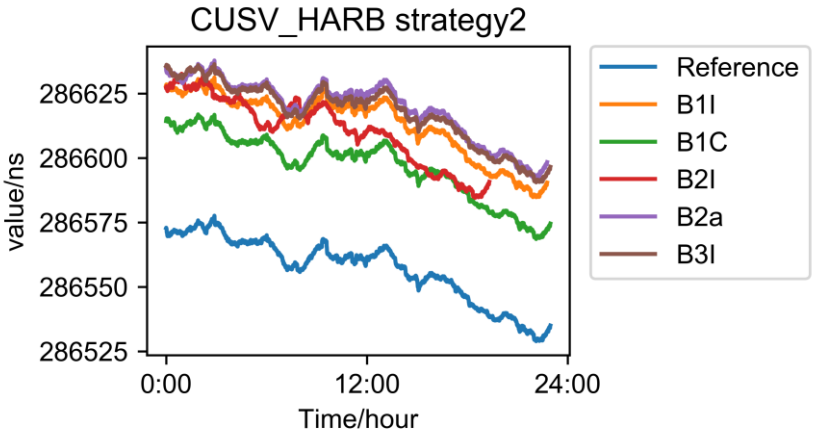

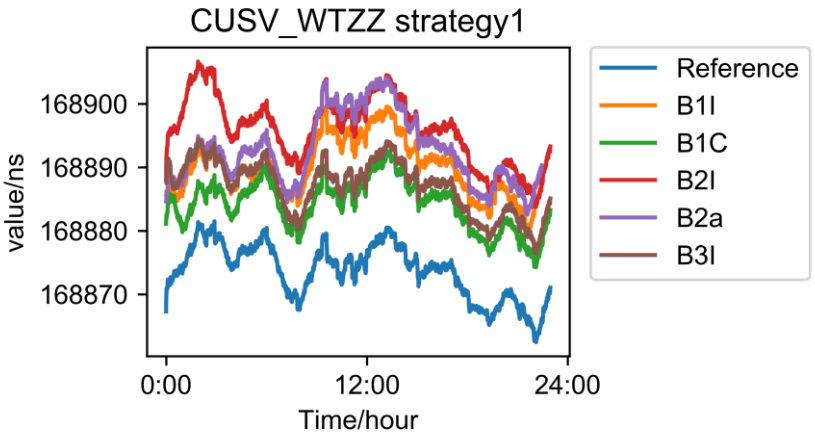

Preprints (www.preprints.org) | NOT PEER-REVIEWED | Posted: 24 October 2022 doi:10.20944/preprints202210.0358.v1

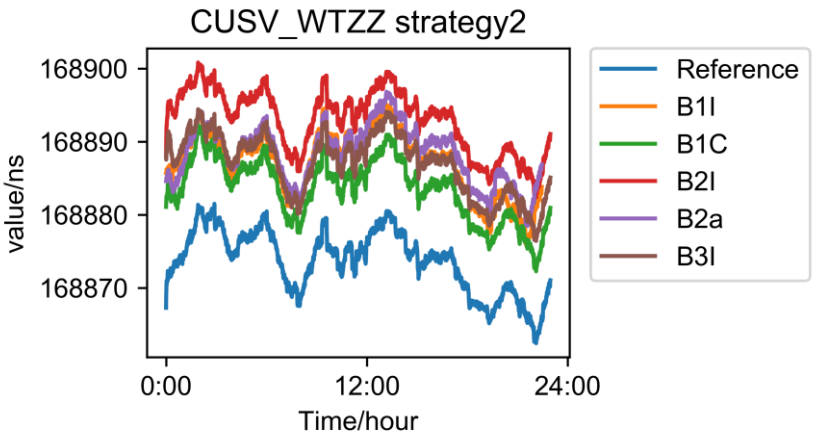

Figure 12. The time sequence diagram of two time-links, two strategies, and 5 frequency points.

Figure 12 shows two time-links sequence of two strategies and 5 frequency. As shown in Figure 12, there was a systematic deviation between the time link of each frequency and the combination of ionosphere free. This systematic deviation originated from two aspects: (1) the system difference between BDS-2 and BDS-3; (2) DCB delay from receiver and satellites, the part of satellite had been corrected, but the part of receiver had not been corrected. The sum of these two parts constitutes the system difference shown in Figure 12.

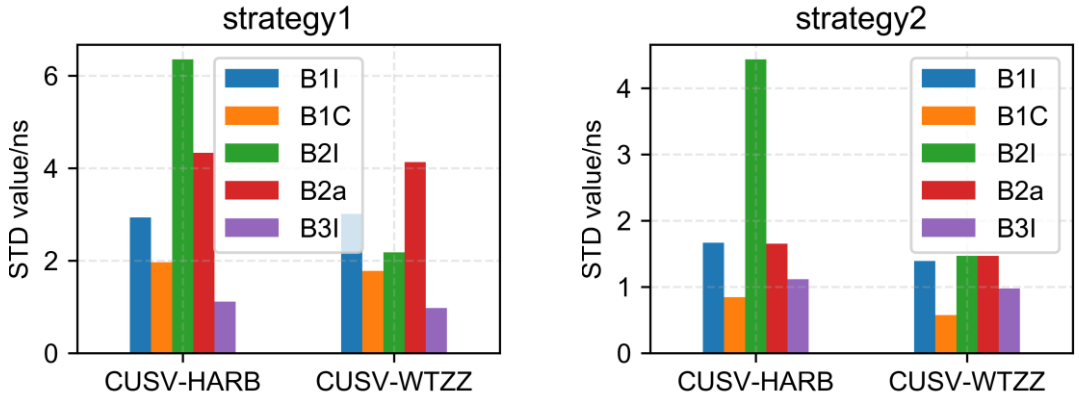

Figure 13. STD of two strategies of time link with 5 frequency.

Taking dual frequency results of B1I and B3I ionosphere free as reference, the single frequency results of 5 frequency were calculated by difference with each other, to obtain STD in Figure 13.

According to the link statistics, the following conclusion can be drawn:

1. The new B1C signal is obviously better than other frequency, while the advantage of B2a signal is not obvious, which may be due to the fewer number of satellites;

2. B3I performs well, which may be due to the large number of satellites. As we know that, BDS-2 and BDS-3 can be used at the same time;

3. B2I performance is worse than others, and the number of satellites is not enough. So, the performances of both links and strategies are worse.

The above is the analysis of time link accuracy. Next, the stability of corresponding time link is analyzed.

Preprints (www.preprints.org) | NOT PEER-REVIEWED | Posted: 24 October 2022 doi:10.20944/preprints202210.0358.v1

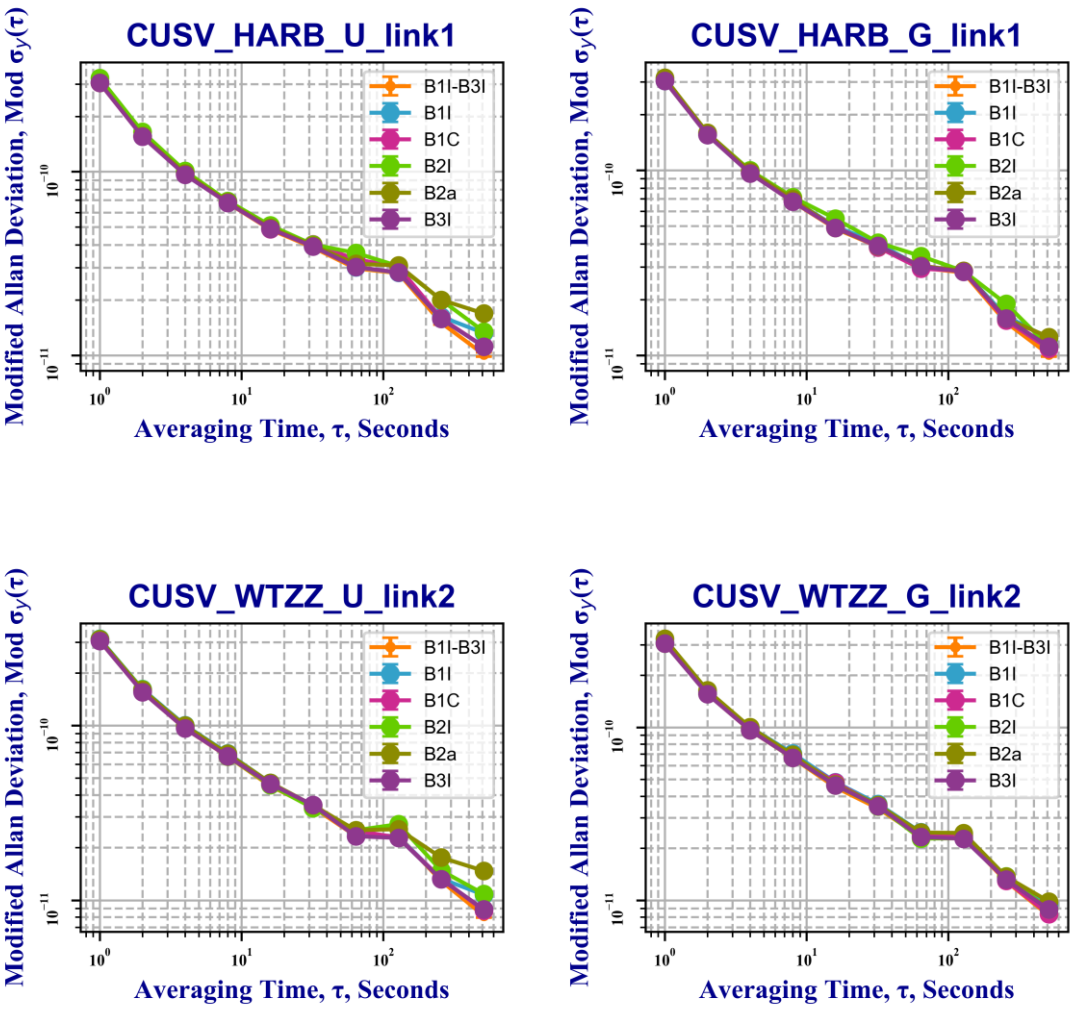

Figure 14. The frequency stability results of the two links of the two strategies (U, strategy1; G, strategy2)

Figures 14 show the statistical results of frequency stability of two strategies links, CUSV-HARB and CUSV- WTZZ links. Based on these results, the following conclusion can be drawn:

1. The frequency stability of two single frequency links can reach the same accuracy as that of dual-frequency;

2. As shown in Figure 14, The stabilities of B1I, B2I, and B2a frequency of strategy 1 are slightly better than those of strategy 1 with averaging time range from 100s to 400s. And we can see that 5 frequency of strategy 2 are closer to the reference value of Reference B1I-B3I.

6. Conclusions

This paper used four types of open service signals (B1I, B1C, B2a, B3I) of the BDS-3 and the B2I signals broadcasted by the BDS-2, to conduct the time transfer and positioning experiments for five types of single frequency signals using the PPP method. Compared with the conventional UC model, a modified GRAPHIC combination was proposed by modifying its stochastic model. The purpose of this paper is to study the needs of the majority of consumer, which are single frequency users, when BDS-2 and BDS-3 coexist at present.

The results of experiment show that:

1. Globally distributed 18 experimental stations can achieve the positioning accuracy of sub-decimeter level with BDS single frequency static PPP method;

2. Compared to the UC method, the modified GRAPHIC method improved the stability and accuracy significantly, and the accuracy of 5 frequency (B1I, B1C, B2I, B2a, and B3I), is increased

 doi:10.20944/preprints202210.0358.v1

40.4%, 32.2%, 80.3%, 12.4%, and 10.3% respectively, when positioning with single frequency PPP method;

3. The single frequency clock difference STD can reach the level of 1 nanosecond; the time transfer link can achieve the STD of about 2 nanoseconds, and the frequency stability of the time transfer link can reach the same accuracy as the combination of the dual-frequency.

Funding: This work was supported by the Key Special Projects of the National Key Research and Development Plan under Grant No. 2018YFB0505200, and the National Natural Science Foundation of China under Grant No. 61973328, No.91938301.

Acknowledgments The authors thank the IGS MGEX for providing the data of multi-GNSS stations, precise orbit, and clock products. Many thanks to the Beidou Science Database of National Space Science Center, Analysis Center of iGMAS National Time Service Center, and iGMAS of Xi'an Data Center.

Conflicts of Interest: The authors declare no conflict of interest.

References

Collins J.P., Langley, Richard Brian, (1997). A tropospheric delay model for the user of the wide area augmentation system. Department of Geodesy and Geomatics Engineering, University of New Brunswick.

CSNO (2018a) BeiDou Navigation satellite system signal in space interface control document open service signal B3I (Version 1.0). China Satellite Navigation Office

Gao, Y.; Shen, X. Improving Ambiguity Convergence in Carrier Phase-Based Precise Point Positioning. Proceedings of the 14th International Technical Meeting of the Satellite Division of The Institute of Navigation (ION GPS 2001), Salt Lake City, UT, USA, 12–14 September 2001; pp. 1532–1539.

Gao, Y. , & Shen, X. . (2002). A new method for carrier-phase-based precise point positioning. Navigation, 49(2), 109-116.

Ge Y, Zhou F, Sun B, Wang S, Shi B (2017) The impact of satellite time group delay and inter-frequency differential code bias corrections on multi-GNSS combined positioning. Sensors 17(3):602

Ge, Y. , Yang, X. , Qin, W. , Su, H. , & Wang, S. . (2018). Time Transfer Analysis of GPS- and BDS-Precise Point Positioning Based on iGMAS Products. China Satellite Navigation Conference (CSNC) 2018 Proceedings.

Ge, Y., Ding, S., Qin, W., Zhou, F., Yang, X., & Wang, S. (2020). Performance of ionospheric-free PPP time transfer models with BDS-3 quad-frequency observations. Measurement, 107836.

Jiao, G. , Song, S. , Ge, Y. , Su, K. , & Liu, Y. . (2019). Assessment of beidou-3 and multi-gnss precise point positioning performance. Sensors, 19(11), 2496-.

Li, X., Yuan, Y., Zhu, Y., Huang, J., Wu, J., Xiong, Y., ... & Li, X. (2019). Precise orbit determination for BDS3 experimental satellites using iGMAS and MGEX tracking networks. Journal of Geodesy, 93(1), 103-117.

Lu, M. , Li, W. , Yao, Z. , & Cui, X. . (2019). Overview of BDS Ⅲ new signals. Navigation, 66(1), 19-35.

Montenbruck O, Steigenberger P, Hauschild A (2018) Multi-GNSS signal-in-space range error assessment–methodology and results. Adv Space Res 61(12):3020–3038

Petit, G., Luzum, B., 2010. IERS conventions (2010) Bureau International Des Poids et Mesures Sevres

 doi:10.20944/preprints202210.0358.v1

(France). (No. IERS-TN-36).

Tu, R. , Zhang, P. , Zhang, R. , Liu, J. , & Lu, X. . (2019). Modeling and performance analysis of precise time transfer based on BDS triple-frequency un-combined observations. Journal of Geodesy, 93(6), 837-847.

Wu, J.T., Wu, S.C., Hajj, G.A., Bertiger, W.I., Lichten, S.M., (1992). Effects of antenna orienation on GPS carrier phase. Manuscr Geod 18, 91–98.

Wang, M. , Wang, J. , Dong, D. , Meng, L. , Chen, J. , & Wang, A. , et al. (2019). Performance of BDS-3: satellite visibility and dilution of precision. Gps Solutions, 23(2).

Wang, N. , Yuan, Y. , Li, Z. , Montenbruck, O. , & Tan, B. . (2016). Determination of differential code biases with multi-gnss observations. Journal of Geodesy, 90(3), 209-228.

Wang, N. , Li, Z. , Montenbruck, O. , & Tang, C. . (2019). Quality assessment of gps, galileo and beidou-2/3 satellite broadcast group delays. Advances in Space Research, 64(9).

Xie, X., Geng, T., Zhao, Q., Cai, H., Zhang, F., Wang, X., & Meng, Y. (2019). Precise orbit determination for BDS-3 satellites using satellite-ground and inter-satellite link observations. Gps Solutions, 23(2), 1-12.

Ye, F., Yuan, Y., & Ou, J. (2018). Initial orbit determination of BDS-3 satellites based on new code signals. Geodesy and Geodynamics, 9(4), 342-346.

Yan, X., Huang, G., Zhang, Q., Liu, C., Wang, L., & Qin, Z. (2019). Early analysis of precise orbit and clock offset determination for the satellites of the global BeiDou-3 system. Advances in Space Research, 63(3), 1270-1279.

Yang, Y. , Gao, W. , Guo, S. , Mao, Y. , & Yang, Y. . (2019). Introduction to beidou-3 navigation satellite system. Navigation.

Yuan, Y. , Wang, N. , Li, Z. , & Huo, X. . (2019). The beidou global broadcast ionospheric delay correction model (bdgim) and its preliminary performance evaluation results. Navigation, 66(1), 55-69.

Zhang, P. , Tu, R. , Gao, Y. , Liu, N. , & Zhang, R. . (2019). Evaluation of carrier-phase precise time and frequency transfer using different analysis centre products for gnsss. Measurement Science & Technology.

Zhang, X. , Wu, M. , Liu, W. , Li, X. , Yu, S. , & Lu, C. , et al. (2017). Initial assessment of the compass/beidou-3: new-generation navigation signals. Journal of Geodesy, 91(10), 1225-1240.

Zhang, Y. , Kubo, N. , Chen, J. , Wang, J. , & Wang, H. . (2019). Initial positioning assessment of BDS new satellites and new signals. Remote Sensing, 11(11), 1320.